 CMC, vol.39, no.3, pp.301-315, 2014

Active Metamaterials for Modulation and Detection

Sameer R. Sonkusale [1], Wangren Xu [1] and Saroj Rout [1]

Abstract: This paper illustrates some new concepts in the area of hybrid metamaterials, which are metamaterials that are embedded with active circuit elements such as transistors. Such transistor/metamaterial hybrids can exhibit some exotic electromagnetic properties which can be exploited for unusual and exciting functions. Two specific examples are provided. In one application, terahertz (THz) modulator based on embedding of psuedomorphic high electron mobility transistor (pHEMT) within the metamaterial resonator, all implemented monolithically in a commercial gallium arsenide (GaAs) technology is presented. In another application, a detector array based on metamaterial perfect absorber for room-temperature detection of gigahertz (GHz) radiation within each sub wavelength metamaterial unit cell is presented. The latter application utilizes a hybridization of metamaterial on printed circuit board (PCB) with discrete microwave electronic components. Both applications indicate the promise of the approach of integrating electronics or semiconductor devices with metamaterials for new and innovative functions.

Keywords: Metamaterials, Active Metamaterials, Terahertz, Imaging.

1 Introduction

Metamaterials are artificially engineeered materials typically consisting of a periodic array of sub-wavelength metallic inclusions in dielectric host substrate that can be made to exhibit exotic electromagnetic properties not readily available in nature [Veselago (1968)]. Metamaterials have been used to demonstrated negative index of refraction [Shelby, Smith and Schultz (2001); Smith, Padilla, Vier, Nemat-Nasser and Schultz (2000)], invisibility cloaks [Schurig, Mock, Justice, Cummer, Pendry, Starr and Smith (2006)], and super lenses [Fang, Lee, Sun and Zhang (2005)]. As metamaterial research continues to mature, a concerted effort to create practical devices that utilize exceptional properties of metamaterials will become increasingly important. This include sources, detectors and modulators for

[1] NanoLab, Electrical and Computer Engineering, Tufts University, 161 College Ave, Medford, MA, 02155, USA.

communication, imaging, and sensing applications. Of special interest has been the achievements made in realizing metamaterials in the *terahertz gap* (0.1-10THz) [Padilla, Aronsson, Highstrete, Lee, Taylor and Averitt (2007); Chen, Padilla, Zide, Gossard, Taylor and Averitt (2006)], where usable naturally occurring materials are somewhat rare making this a challenging area to build traditional electronic or photonic devices. Another area of specific interest has been to make detectors or focal plane arrays based on metamaterials that can provide imaging capabilities in the challenging millimeter wave and terahertz region of the electromagnetic spectrum.

Research activities from our group have focused on making hybrid metamaterials containing active circuit elements such as transistors. Such transistor/metamaterial hybrids can exhibit some exotic electromagnetic properties not typically possible with conventional metamaterials. Below we discuss two specific examples of applications that explore interactions of active semiconductor devices and circuits with metamaerial resonator structures for exciting functions of modulation and detection. In one application, terahertz THz modulator based on embedding of psuedomorphic high electron mobility transistor (pHEMT) within the metamaterial resonator, all implemented monolithically in a commercial gallium arsenide (GaAs) technology is presented. In another application, a detector array based on metamaterial perfect absorber (MPA) for room-temperature detection of gigahertz (GHz) radiation within each sub wavelength metamaterial unit cell is presented. The latter utilizes a hybridization of metamaterial on printed circuit board (PCB) with discrete microwave electronic components. Both applications indicate the promise of integrating electronics or semiconductor devices with metamaterials for new and innovative functions.

2 Hybrid HEMT/Metamaterial Based Terahertz Modulator

Most metamaterial demonstrations in the literature are with unit cells that are essentially passive resonators. However real practical applications for modulators and detectors require that metamaterial response can be tuned or change in response to stimuli. Tuning for example can provide frequency and phase modulation, and so far approaches for doing that have relied on photodoping, electronic control [Chen, Padilla, Zide, Gossard, Taylor and Averitt (2006)] and temperature effects [Driscoll, Palit, Qazilbash, Brehm, Keilmann, Chae, Yun, Kim, Cho, Jokerst, Smith and Basov (2008)]. In photodoping, the charge carrier concentration in the host dielectric medium is adjusted by high powered optical beams. In temperature responsive metamaterials, novel phase change materials such as vanadium oxide that have temperature dependent insulator to metal transition (or vice versa) is used. However, both of these approaches are not truly scalable. Optical doping needs high powered light sources and bulky optical equipment, while

phase change material based on emerging materials are still not commercially viable for large scale manufacturing. We believe that electronic control using solid state semiconductor devices [Chen, Padilla, Zide, Gossard, Taylor and Averitt (2006)] are the only viable alternative owing to the low cost and relatively mature processing afforded by semiconductor manufacturing. Prior demonstrations have included Schottky diodes which are electronically biased in forward or reverse bias for on-off control to achieve amplitude modulation [Chen, Padilla, Zide, Gossard, Taylor and Averitt (2006); Chen, Palit, Tyler, Bingham, Zide, O'Hara, Smith, Gossard, Averitt, Padilla, Jokerst and Taylor (2008); Paul, Imhof, Lagel, Wolff, Heinrich, Hofling, Forchel, Zengerle, Beigang and Rahm (2009)], and controlling the amount of forward bias can achieve fine amplitude [Chen, Padilla, Zide, Gossard, Taylor and Averitt (2006); Chen, Palit, Tyler, Bingham, Zide, O'Hara, Smith, Gossard, Averitt, Padilla, Jokerst and Taylor (2008)] and also phase modulation [Chen, Padilla, Cich, Azad, Averitt and Taylor (2009)]. We recently demonstrated a hybrid HEMT/metamaterial device that utilizes monolithic integration of transistors at the metamaterial unit cell level and is able to perform as an intensity modulators at terahertz frequencies with switching speeds up to 10 MHz [Shrekenhamer, Rout, Strikwerda, Bingham, Averitt, Sonkusale and Padilla (2011)]. This example is reviewed in the section below in a bit more detail.

2.1 Design

A commercial GaAs technology with three metal layers, an enhanced mode pseudomorphic HEMT, and a silicon nitride encapsulating dielectric layer was used to make the modulator see Fig. 1 [Shrekenhamer, Rout, Strikwerda, Bingham, Averitt, Sonkusale and Padilla (2011)]. The metamaterial geometry is based on the electric split-ring resonator (ESRR) [Padilla, Aronsson, Highstrete, Lee, Taylor and Averitt (2007); Schurig, Mock and Smith (2006)] shown in Fig.1(a). Each unit cell consists of two single rings butted together with their split gaps at the outside. The line width of the metamaterial is 4μm and the split gap is 3 μm. The metamaterial had the dimensions of 42 μm wide by 30 μm in height. A periodic array of these unit cells as shown in Fig.1(b) was fabricated, with period of 55 μm $\times$ 40μm, and a total size of 2.75 $\times$ 2.6 mm^2 with 3200 elements total. Metamaterial elements are fabricated on a $100\mu m$ thick semi-insulating (SI) GaAs substrate. Please note that the geometry and layout is restricted by the design rules specific to the semiconductor technology that dictate minimum spacing and dimensions for each layer in the technology. This not only puts a fundamental limit on the dimensions but also on the geometry of the resonator chosen. Migrating to newer semiconductor technologies with much finer resolution for sizing and spacing can allow scaling to higher frequencies.

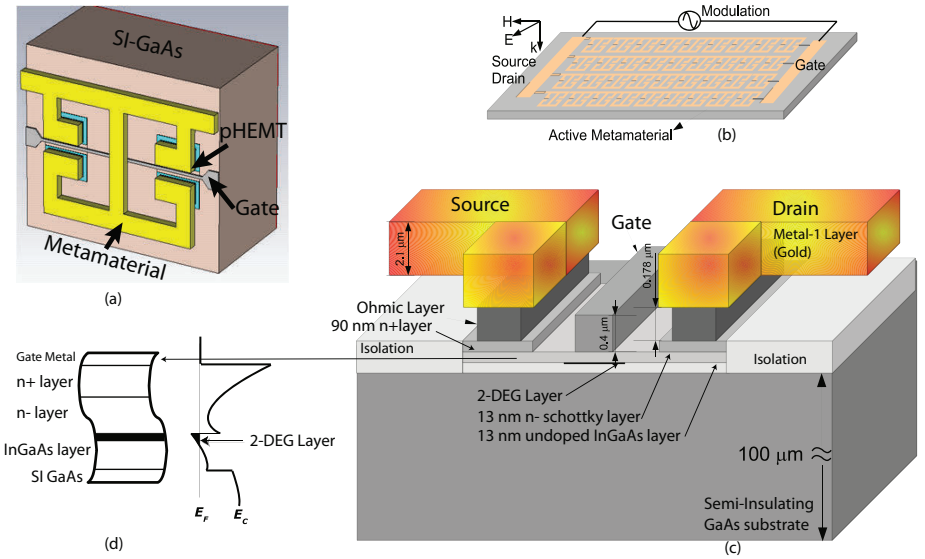

Figure 1: (Color online) Hybrid HEMT/metamaterial THz modulator. (a) Single unit cell. (b) Schematic of the entire HEMT / metamaterial device (c) Cross-sectional at the split gap (d) Band diagram detailing the 2DEG layer in the undoped In-GaAs at the interface with the Schottky layer. Reprinted from [Shrekenhamer, Rout, Strikwerda, Bingham, Averitt, Sonkusale and Padilla (2011)]

A HEMT lies underneath each of the split gaps of the metamaterial element, (two per unit cell), as shown in cross-section in Fig.1(c). The gate length is $0.5\mu m$ and has a width $5\mu m$ for each device. The HEMT consists of pseudomorphic undoped In-GaAs and a lightly doped Schottky layer, of 13 nm thickness forming a heterojunction. A 2DEG is formed in the undoped In-GaAs channel layer as predicted by the band diagram at the interface (Fig.1(d)). Unlike traditional FETs, this channel is formed in an intrinsic (undoped) crystal, resulting in very high mobility ($\sim 6000\ \mathrm{cm}^2/V \cdot s$) and charge density ($\sim 3 \times 10^{12}\mathrm{cm}^{-2}$) at room temperature, thus enabling fast conduction even at THz frequencies.The source and drain are shorted through the metamaterial as a direct consequence of the metamaterial structure we have selected.

The same metal layer which is used to form each metamaterial is also used to connect each element together within the same row. These wires run perpendicular to the split gaps; the incident electric field is also aligned in the direction of the split gap. Single bond pad conects to all the transistor along the perimiter to provide DC

bias voltage for the drain and source of the HEMT. The gates for all HEMTs are connected in a similar fashion to a single bond pad which provides the DC bias voltage for the gate.

2.2 Results and Discussion

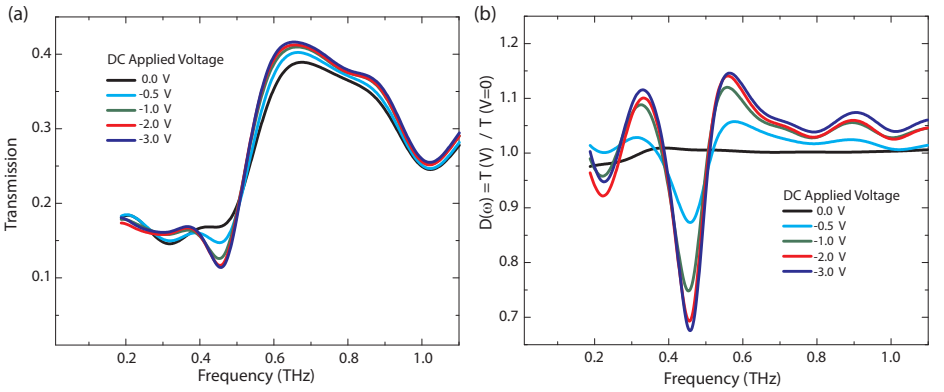

Figure 2: (Color online) (a) Absolute transmission of electric field and (b) Differential transmission with respect to zero bias, both as a function of bias voltage. Reprinted from [Shrekenhamer, Rout, Strikwerda, Bingham, Averitt, Sonkusale and Padilla (2011)]

THz-TDS [Paul, Imhof, Lagel, Wolff, Heinrich, Hofling, Forchel, Zengerle, Beigang and Rahm (2009); Cai, Brener, Lopata, Wynn, Pfeiffer, Stark, Wu, Zhang and Federici (1998)] was used to characterize the device using incident THz electric field ($\vec{E}_i(t)$) polarized along the direction of the split gap of the metamaterial. At the resonant frequency of the metamaterial, (0.46 THz), the electric field is concentrated within the split gaps of the metamaterial. In Fig. 2(a) we show the transmitted electric field as a function of frequency for different V_{GS} values. For V_{GS} less than $-1.0V$, the channel is completely depleted, and transmission shows a resonance at 0.46 THz. When the gate-to-source voltage is increased above $-1.0V$, the channel starts forming between the split gaps, and the metamaterial resonance begins to diminish. At $V_{GS} = 0V$, when the channel is completely formed, a low-impedance path at the split gap is created which effectively shorts the metamaterial resonant response. It can be seen in the transmission data (Fig.2(a)) that the frequency response shows no resonance at $V_{GS} = 0V$. The differential transmission, defined as $D(\omega) = T(\omega)_{V_{GS}}/T(\omega)_{V_{GS}=0V}$ is shown in Fig. 2 showcasing the same results that

clearly show the maximum index of modulation at resonance [Shrekenhamer, Rout, Strikwerda, Bingham, Averitt, Sonkusale and Padilla (2011)].

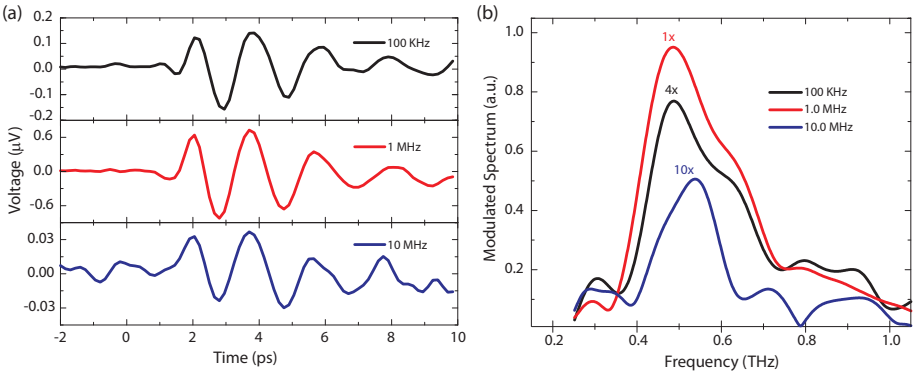

Figure 3: (Color online) (a) Time domain data and (b) Spectra for modulation at frequencies of 100 Hz, 1 MHz and 10 MHz. Reprinted from [Shrekenhamer, Rout, Strikwerda, Bingham, Averitt, Sonkusale and Padilla (2011)]

For high speed dynamic modulation, we utilize the same THz-TDS setup but instead of using a standard mechanical chopper, we replace it with the HEMT / metamaterial modulator. The only difference compared to mechanical chopper is that this only allows a narrow band of frequencies about the metamaterial resonance to be modulated. A square-wave bias, alternating between -1.1 V and 0 V, was applied to the gate of the HEMT with respect to the source and drain. The same square wave signal was applied to the reference input of the lock-in amplifier. The time-domain signal $V_{out}(t)$ is plotted in Fig.3 (a) for three different modulation frequencies, 100 kHz, 1 MHz and 10 MHz and fourier transform of this waveform is plotted in Fig.3 (b). It can be seen that the peak of the spectrum lies at 0.46 THz indicating modulation of the metamaterial resonance. The modulation amplitude falls off at higher modulating frequencies above 10 MHz. This is attributed to the parasitic nature of the long bond wires used in the chip assembly and, is not a limitation of either the HEMT or metamaterial device [Shrekenhamer, Rout, Strikwerda, Bingham, Averitt, Sonkusale and Padilla (2011)]. One can be expected to get modulation close to the maximum frequency of the transistor in a given GaAs technology.

3 Metamaterial Focal Plane Array Imager

While the previous section discussed the possibility of embedding transistors or active devices inside metamaterial unit cells to control and tune their response, another possibility could be to place electronic devices inside metamaterial constructs in order to sense or harvest the metamaterial response to incident radiation. In this section, we review our recent work of designing a metamaterial perfect absorber (MPA) and its utilization as a metamaterial detector and collectively as a focal plane array [Shrekenhamer, Xu, Venkatesh, Schurig, Sonkusale and Padilla (2012); Venkatesh, Shrekenhamer, Xu, Sonkusale, Padilla and Schurig (2013)]. The ability of metamaterial unit cells to completely absorb incident electromagnetic energy – with effectively zero reflected signal in MPA realization – has been demonstrated across much of the electromagnetic spectrum [Landy, Sajuyigbe, Mock, Smith and Padilla (2008); Tao, Landy, Bingham, Zhang, Averitt and Padilla (2008); Hao, Wang, Liu, Padilla, Zhou and Qiu (2010)]. One key design feature afforded by metamaterials is the ability to engineer materials with a specified electric $[\varepsilon(\omega)]$ and magnetic $[\mu(\omega)]$ response. This allows for matching the impedance $Z(\omega) = \sqrt{\mu(\omega)/\varepsilon(\omega)}$ of the MPA to that of free space. We decide to utilize the excellent absorbing capability of MPA to harvest the incident electromagnetic energy at resonance with high efficiency for detection. The device is designed for RF frequencies, because the dimensions of the metamaterial unit cells are in millemeters and embedding of electronic devices to interface with this antenna is more favorable from practical standpoint [Shrekenhamer, Xu, Venkatesh, Schurig, Sonkusale and Padilla (2012); Venkatesh, Shrekenhamer, Xu, Sonkusale, Padilla and Schurig (2013)]. Utilizing semiconductor technology for monolithic integration as described in previous section will allow one to scale to optical frequencies as well.

3.1 Design

In essence, each metamaterial unit cell functions as an individual antenna coupled detector and, collectively, as a focal plane array. The metamaterial unit cell converts the incident microwave radiation into voltage/current signals that are guided to dedicated microwave receiver chain and finally detected with microwave power detector to produce DC voltage linearly proportional to the microwave signal [Shrekenhamer, Xu, Venkatesh, Schurig, Sonkusale and Padilla (2012)]. In another realization [Venkatesh, Shrekenhamer, Xu, Sonkusale, Padilla and Schurig (2013)], the signal is routed to coherent receiver for measuring both intensity and phase. We will focus mostly on intensity measurements using power detectors as described in [Shrekenhamer, Xu, Venkatesh, Schurig, Sonkusale and Padilla (2012)]. 11 x 11 metamaterial elements and receiver system components are integrated into a single

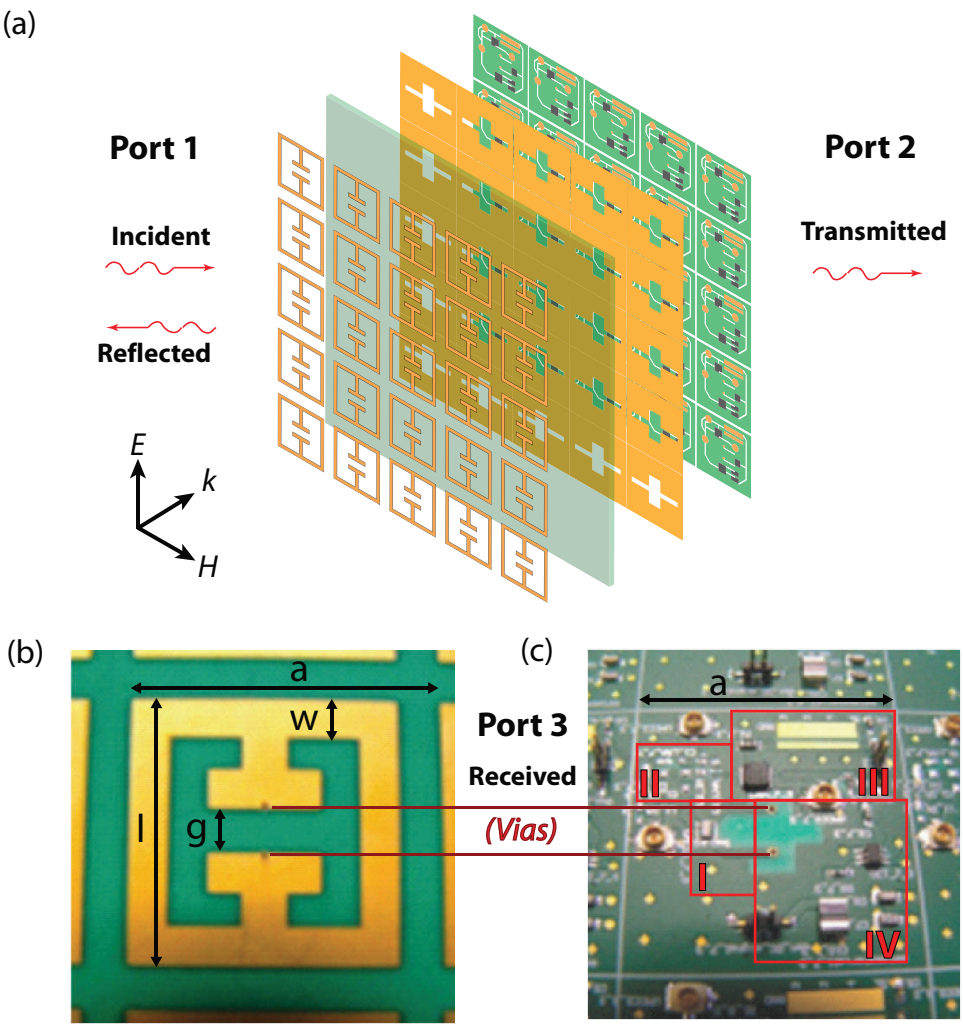

Figure 4: (Color online) Metamaterial focal plane array architecture. (a) Schematic of the full device with layers shown from top to bottom are: the electrical LC resonator, Rogers dielectric spacer, patterned ground plane, and microwave power receiver circuit. Port 1 and 2 shown(b) Photo of an individual pixel, i.e. an ELC unit cell with dimensions of $a = 27.3$, $l = 24$, $w = 3.5$, and $g = 4$; all in millimeters. (c) Photo of the circuit layer with *vias* indicated. The *vias* transport the received signal (port 3) to the microwave power receiver circuit underneath each unit cell where the different highlighted regions are: (I) balun, (II) impedance matching circuit, (III) low noise amplifier, and IV) microwave power detector. Reprinted from [Shrekenhamer, Xu, Venkatesh, Schurig, Sonkusale and Padilla (2012)]

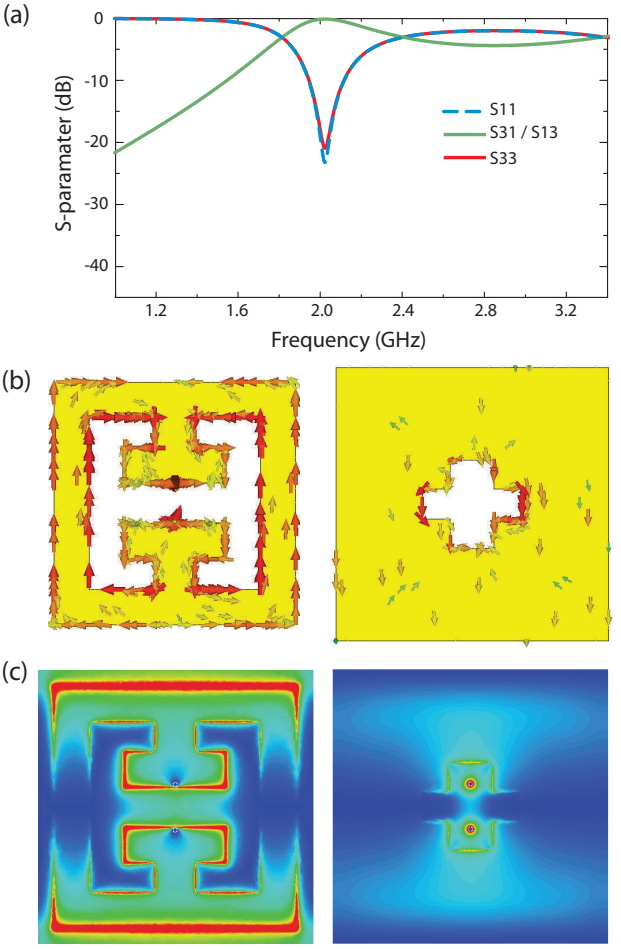

Figure 5: (Color online) FDTD simulation of the metamaterial detector. (a) Free space reflection (S_{11} dashed blue curve), transmission (S_{31} green curve), and reflection coefficient (S_{33} red curve). Simulated current densities (b) and electric field magnitude (c) shown directly underneath the ELC (left) and above the ground plane (right) at the simulated design frequency of 2.0 GHz. Reprinted from [Shrekenhamer, Xu, Venkatesh, Schurig, Sonkusale and Padilla (2012)]

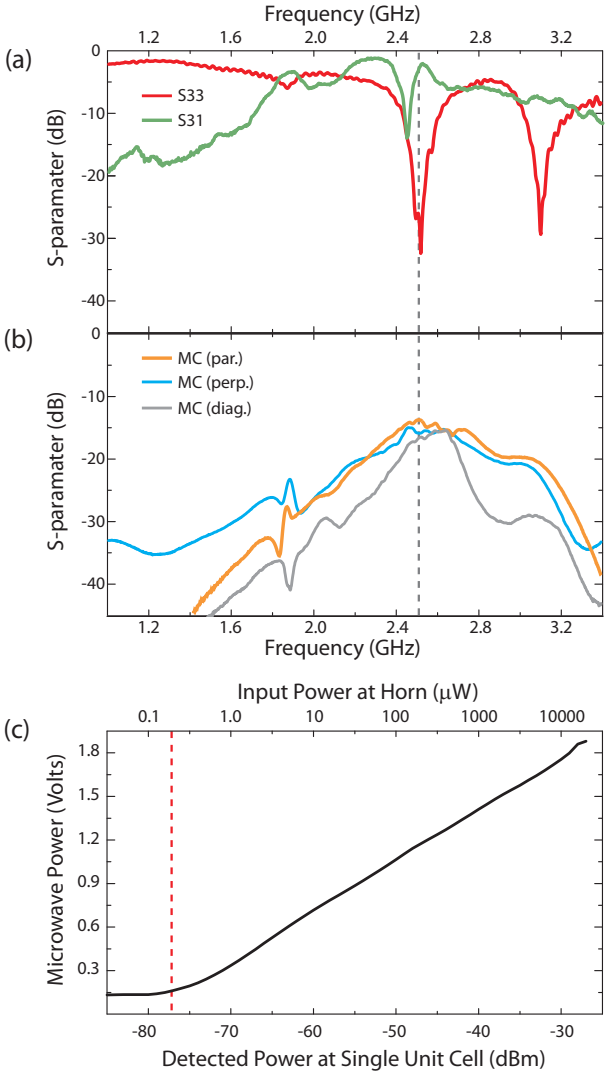

Figure 6: (Color online) Experimental measurements for the center pixel in the focal plane array. (a) S- parameter data shows the reflection coefficient (S_{33} red curve) and the transmission (S_{31} green curve) with the dashed grey line at 2.5 GHz (b) Mutual coupling (MC) between neighboring metamaterial pixels located parallel (gold curve), perpendicular (blue curve), and diagonal (grey curve) with respect to the electric field polarization. (c) Sensitivity characterization with the output of microwave power detector of single pixel as function of incident power, and is sensitive as indicated by dashed red line down to -77 dBm at 2.5 GHz. Reprinted from [Shrekenhamer, Xu, Venkatesh, Schurig, Sonkusale and Padilla (2012)]

four layer printed circuit board (PCB) as shown in Fig.4. All the blocks shown in Fig.4 are contained within each unit cell – consists of the ELC resonator followed by a balun, impedance matching circuit, Low Noise Amplifier (LNA) and a microwave power detector. Beginning from the side of the detector where microwave radiation is incident, the first layer contains the Electrically coupled LC resonator (ELC resonator) based metamaterial array [Schurig, Mock and Smith (2006)], the second layer is made of a ground plane, third layer is a power routing plane, and then finally the backside is a circuit layer. Each metal layer is separated by Rogers 4003 dielectric core with prepreg. Microwave radiation received by the ELC resonator is transferred by a pair of through-hole *vias* to the circuit layer where the balun is used to transform the balanced signal to unbalanced signal. The unbalanced signal is then fed into an impedance matching circuit which, not only maximizes the signal power transfer from ELC resonator to microwave receiver chain, but also compensates for variantions in the ELC resonator's resonance frequency due to fabrication tolerances. Finally the signal is amplified by the Low Noise Amplifier (LNA) before being converted to a DC signal by the microwave power detector for intensity imaging [Shrekenhamer, Xu, Venkatesh, Schurig, Sonkusale and Padilla (2012)] (or a coherent receiver for combined intensity/phase imaging [Venkatesh, Shrekenhamer, Xu, Sonkusale, Padilla and Schurig (2013)]).

3.2 Results and Discussion

The design flow uses a combination of finite difference time domain (FDTD) simulation using CST Microwave Studio and circuit simulation using Agilent ADS design environment. Ports are defined as shown in Fig. 4. The simulated scattering parameters are shown in Fig. 5(a). It demonstrates that a maximum in transmission corresponds with the minima of both reflection coefficients S_{11} and S_{33} at 2.0 GHz. Value of S_{31}= 0.986 indicates that over 97% of the incident intensity is transmitted into the detector circuit. In Fig. 5(b) shows the surface current density at resonance and Fig. 5(c) shows the magnitude of the electric field which shows that the electric field is focused into the ELC split gap (right panel) and the *vias* are sufficiently decoupled from the ground plane.

An important observation from this work was that variations in component values and the geometry can occur in the fabrication process and may alter the ideal electromagnetic response. The measured S_{33} shown as the red curve in Fig. 6(a) is at 2.5 GHz which is not the same as the simulated minimum in S_{33} which occurs at 2.0 GHz. Free space measurements of the center pixel were performed within an anechoic chamber with all neighboring unit cells having 50 Ω terminations following their respective balun output connections. The metamaterial array was placed 1.75 m away from the horn antenna to be in the far field of the horn's radiating field

pattern. In Fig. 6(a), the green S_{31} curve shows a peak about 2.5 GHz overlapping with the minimum observed in S_{33} as expected. The gold curve in Fig. 6(b) displays the measured mutual coupling (MC) between neighboring unit cells parallel, perpendicular and diagnoal to the electric field direction. Values of MC are significantly low, especially considering the proximity of nearest neighbors at a lattice spacing of λ/4.4 (27.3 mm) and with edge separation of λ/40 (3.0 mm). This is a significant result since it indicates that one can pack metamaterial resonator antennas in close geometry without interference between them, and this is quite ideal for multiple input multiple output (MIMO) communication applications. It should be mentioned that polarization measurements were also performed and the results were consistent with expectations that signal polarized along the direction of split gap is necessary to get the responses shown in Fig.6 [Shrekenhamer, Xu, Venkatesh, Schurig, Sonkusale and Padilla (2012)].

In another related work, the power detector was replaced with low-IF coherent receiver chain to perform vector measurements [Venkatesh, Shrekenhamer, Xu, Sonkusale, Padilla and Schurig (2013)]. In this demonstration, sources with power outputs typical of mobile/wireless devices (about -24 dBm) could be resolved at a kilometer distance away with sub-degree resolution, essentially outperforming the traditional phased array spaced at $\lambda/2$ apart at low SNRs. This is a unique application where metamaterial array has been employed for direction finding based on intensity/phase measurements [Venkatesh, Shrekenhamer, Xu, Sonkusale, Padilla and Schurig (2013)].

4 Conclusion

In this article we presented two examples from our research group on hybrid integration of electronic devices and circuits inside metamaterial structures.

In one application, we demonstrated a HEMT / metamaterial device capable of modulation of THz radiation at frequencies up to 10 MHz, and modulation depths of up to 33% at 0.46 THz with all electronic control using a commercial GaAs technology. We achieved monolithic integration of a total of 2×10^4 active transistors at the metamaterial unit cell level. Thus hybrid HEMT/metamaterial structures are ideal for making modulators for the challenging terahertz spectrum.

In another application, we demonstrated a metamaterial absorber based focal plane array to operate at 2.5 GHz which showed a very have high pixel sensitivity of -77 dBm in addition to low pixel to pixel coupling interference below -14 dB, very good frequency selectivity and wide angular performance. The proposed metamaterial absorber configuration has the ability to capture nearly all of the incident electromagnetic energy at design frequencies across the entire electromagnetic spectrum

and therefore could be utilized within detector pixels as part of bolometric or semiconducting detectors as well. The sub-wavelength unit cell geometry and narrow resonant spectral bandwidth that is also polarization sensitive makes a case for the possibility of making hyper- or multi-spectral, polarization-sensitive focal plane array imagers.

We note that both the applications listed here are not restricted to the frequency applied but could be scaled to other frequencies, even much higher closer to the optical spectrum, on account of continuous scaling of semiconductor technology on which they will be implemented.

Acknowledgement: The modulator work was done in collaboration with Boston College (Dr. Willie Padilla, Dr. David Shrekenhamer) and the detector work was also done in collaboration with University of Utah (Dr. David Schurig, Suresh Venkatesh) through the funding from National Science Foundation (NSF) grants ECCS-1002340 and ECCS-1002152 and Office of Naval Research grants N00014-09-1-1075.

References

Cai, Y.; Brener, I.; Lopata, J.; Wynn, J.; Pfeiffer, L.; Stark, J. B.; Wu, Q.; Zhang, X. C.; Federici, J. F. (1998): Coherent terahertz radiation detection: Direct comparison between free-space electro-optic sampling and antenna detection. *Applied Physics Letters*, vol. 73, no. 4, pp. 444–446.

Chen, H. T.; Padilla, W. J.; Cich, M. J.; Azad, A. K.; Averitt, R. D.; Taylor, A. J. (2009): A metamaterial solid-state terahertz phase modulator. *Nature Photonics*, vol. 3, no. 3, pp. 148–151.

Chen, H. T.; Padilla, W. J.; Zide, J. M. O.; Gossard, A. C.; Taylor, A. J.; Averitt, R. D. (2006): Active terahertz metamaterial devices. *Nature*, vol. 444, no. 7119, pp. 597–600.

Chen, H. T.; Palit, S.; Tyler, T.; Bingham, C. M.; Zide, J. M. O.; O'Hara, J. F.; Smith, D. R.; Gossard, A. C.; Averitt, R. D.; Padilla, W. J.; Jokerst, N. M.; Taylor, A. J. (2008): Hybrid metamaterials enable fast electrical modulation of freely propagating terahertz waves. *Applied Physics Letters*, vol. 93, no. 9.

Driscoll, T.; Palit, S.; Qazilbash, M. M.; Brehm, M.; Keilmann, F.; Chae, B. G.; Yun, S. J.; Kim, H. T.; Cho, S. Y.; Jokerst, N. M.; Smith, D. R.; Basov, D. N. (2008): Dynamic tuning of an infrared hybrid-metamaterial resonance using vanadium dioxide. *Applied Physics Letters*, vol. 93, no. 2.

Fang, N.; Lee, H.; Sun, C.; Zhang, X. (2005): Sub-diffraction-limited optical imaging with a silver superlens. *Science*, vol. 308, no. 5721, pp. 534–537.

Hao, J. M.; Wang, J.; Liu, X. L.; Padilla, W. J.; Zhou, L.; Qiu, M. (2010): High performance optical absorber based on a plasmonic metamaterial. *Applied Physics Letters*, vol. 96, no. 25.

Landy, N. I.; Sajuyigbe, S.; Mock, J. J.; Smith, D. R.; Padilla, W. J. (2008): Perfect metamaterial absorber. *Physical Review Letters*, vol. 100, no. 20.

Padilla, W. J.; Aronsson, M. T.; Highstrete, C.; Lee, M.; Taylor, A. J.; Averitt, R. D. (2007): Electrically resonant terahertz metamaterials: Theoretical and experimental investigations. *Physical Review B*, vol. 75, no. 4.

Paul, O.; Imhof, C.; Lagel, B.; Wolff, S.; Heinrich, J.; Hofling, S.; Forchel, A.; Zengerle, R.; Beigang, R.; Rahm, M. (2009): Polarization-independent active metamaterial for high-frequency terahertz modulation. *Optics Express*, vol. 17, no. 2, pp. 819–827.

Schurig, D.; Mock, J. J.; Justice, B. J.; Cummer, S. A.; Pendry, J. B.; Starr, A. F.; Smith, D. R. (2006): Metamaterial electromagnetic cloak at microwave frequencies. *Science*, vol. 314, no. 5801, pp. 977–980.

Schurig, D.; Mock, J. J.; Smith, D. R. (2006): Electric-field-coupled resonators for negative permittivity metamaterials. *Applied Physics Letters*, vol. 88, no. 4.

Shelby, R. A.; Smith, D. R.; Schultz, S. (2001): Experimental verification of a negative index of refraction. *Science*, vol. 292, no. 5514, pp. 77–79.

Shrekenhamer, D.; Rout, S.; Strikwerda, A. C.; Bingham, C.; Averitt, R. D.; Sonkusale, S.; Padilla, W. J. (2011): High speed terahertz modulation from metamaterials with embedded high electron mobility transistors. *Optics Express*, vol. 19, no. 10, pp. 9968–9975.

Shrekenhamer, D.; Xu, W. R.; Venkatesh, S.; Schurig, D.; Sonkusale, S.; Padilla, W. J. (2012): Experimental realization of a metamaterial detector focal plane array. *Physical Review Letters*, vol. 109, no. 17.

Smith, D. R.; Padilla, W. J.; Vier, D. C.; Nemat-Nasser, S. C.; Schultz, S. (2000): Composite medium with simultaneously negative permeability and permittivity. *Physical Review Letters*, vol. 84, no. 18, pp. 4184–4187.

Tao, H.; Landy, N. I.; Bingham, C. M.; Zhang, X.; Averitt, R. D.; Padilla, W. J. (2008): A metamaterial absorber for the terahertz regime: Design, fabrication and characterization. *Optics Express*, vol. 16, no. 10, pp. 7181–7188.

Venkatesh, S.; Shrekenhamer, D.; Xu, W. R.; Sonkusale, S.; Padilla, W.; Schurig, D. (2013): Interferometric direction finding with a metamaterial detector. *Applied Physics Letters*, vol. 103, no. 25.

Veselago, V. G. (1968): Electrodynamics of substances with simultaneously negative values of sigma and mu. *Soviet Physics Uspekhi USSR*, vol. 10, no. 4, pp. 509–514.